International Journal of Offshore and Polar Engineering (ISSN 1053-5381)

Vol. 15, No. 1, March 2005, pp. 1–7

# Optimization of Vortex Shedding in 3-D Wakes Using Belt Actuators

Philippe Poncet
Laboratory Mathematics for Industry and Physics, National Institute of Applied Sciences (INSA)
Toulouse, France

Petros Koumoutsakos
Institute of Computational Science, Swiss Federal Institute of Technology, Zurich, Switzerland

**This paper discusses the control of cylinder wakes via tangential wall velocity modifications. The wall velocity is piecewise constant (corresponding to belt actuators), and its amplitude is optimized using a clustering real coded genetic algorithm. This type of control significantly affects the vortical structures being shed in the wake, and it is shown that the flow gets significantly modified, resulting in a 3-dimensional body shedding 2-dimensional vortical structures.**

## INTRODUCTION

We are interested in the manipulation of vortex shedding of 3-D wakes and the associated drag reduction in the canonical case of a 3-D cylinder. Control is performed by means of tangential velocities on the body, which in practice can be translated as wall parallel belt actuators or tangential local jets. We develop suitable numerical methods to solve numerically the 3-D Navier-Stokes equations and implement clustering genetic algorithms in order to optimize the actuator parameters.

In order to compute these flows accurately, we developed a vortex-in-cell method using a coupling between grids and particle. Vortex methods make the nonlinearity of the transport terms vanish from the Navier-Stokes equation, thus alleviating the related stability condition usually encountered in Eulerian schemes that can be very restrictive on the time-step. This advantage of the Lagrangian method is counterbalanced by a lack of accuracy, especially for vortex methods based on random walks. The coupling between particles and grids permits the overcoming of this difficulty as well as the reduction of the computational cost of evaluating the velocity field (even when compared to multipoles methods for the Biot-Savart laws). The associated integrals and derivative operators can be computed with good accuracy. This has been validated in Cottet and Koumoutsakos (2000), Cottet and Poncet (2002, 2003, 2004), and Poncet (2002, 2004).

In order to perform a control by means of a tangential wall velocity (belt actuators), we first consider the 2-D problem. This has been obtained by a genetic algorithm, whose histogram and most probable solution are in Milano and Koumoutsakos (2002) and in this paper.

This 2-D profile of velocity is then fitted by a smooth symmetric function and applied on 3-D flows. (See the article by Poncet, Cottet and Koumoutsakos, to appear in *C. R. Mécanique.*) In these 3-D simulations one can observe the behavior of 3-dimensionality, the drag reduction and shedding cancellation (in the sense of force oscillation, i.e., drag and mean vorticity variations). One can also check that the property of shedding reduction is still valid when a full 3-D profile of velocity is applied on the body.

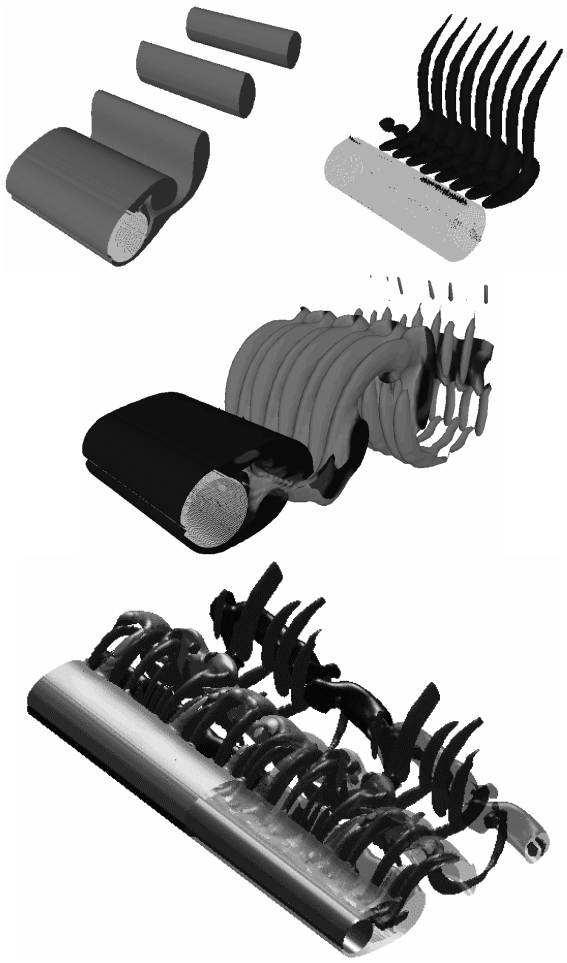

Fig. 1 Dynamics of cylinder wake in 3-D at Re = 300: 2-D wake (top left), first signature of instability (top right), resultant 3-D wake before saturation (middle), and post-transient established 3-D flow with fully developed hydrodynamic instabilities (bottom, from Poncet, 2004)

Received August 24, 2004; revised manuscript received by the editors December 15, 2004. The original version (prior to the final revised manuscript) was presented at the 14th International Offshore and Polar Engineering Conference (ISOPE-2004), Toulon, France, May 23–28, 2004.

KEY WORDS: Shedding manipulation, genetic algorithms, 3-D wakes, vortex methods, hydrodynamic instabilities.

## NUMERICAL APPROACH

We consider the 3-D Navier-Stokes equations in their velocity-vorticity formulation:

$$\frac{\partial \omega}{\partial t} + u \cdot \nabla \omega - \omega \cdot \nabla u - \nu \Delta \omega = 0 \tag{1}$$

where $\omega$ is the vorticity field, $u$ the velocity field, and $\nu$ the kinematic viscosity. This equation is defined over a cylindrical domain, around a cylinder of diameter $D$ ($R = D/2$ will denote the radius) and spanwise length $L$. One considers $L$-periodic solutions. The far field condition on velocity is $U \to U_\infty \mathrm{e}_x$ where $\mathrm{e}_x$ is the streamwise basis vector.

Further, the relation $\omega = \mathrm{curl}\, u$ is satisfied for all time, as well as the incompressibility $\mathrm{div}\, u = 0$ and the no-slip condition $u = 0$ on the body.

The Reynolds number $\mathrm{Re} = U_\infty D/\nu$ gives information on the flow nature (steady, oscillatory, 3-D unstable, turbulent, etc.) In the present simulations, one has Re = 300 for 3-D simulations and 500 for 2-D simulations.

The numerical method used to solve the Navier-Stokes Eq. 1 is a hybrid vortex method, joined to a time-splitting algorithm for convection and diffusion. One considers the vorticity field in its Lagrangian formulation:

$$\omega(t) = \sum_{p=1}^{n} \omega_p(t) \delta_{x_p(t)} v_p \tag{2}$$

where $\omega_p(t)$ is the particle vorticity, $x_p(t)$ the characteristic curve, and $v_p$ the volume of the particle (which remains constant in time due to the incompressibility). The time-splitting algorithm is described below.

### Lagrangian Convection Step

The convection part can thus be written as:

$$\begin{cases} \dfrac{d\omega_p}{dt} = \omega \cdot \nabla u(x_p) \\ \dfrac{dx_p}{dt} = u(x_p) \\ \dfrac{dv_p}{dt} = v_p\ \mathrm{div} u(x_p) = 0 \end{cases} \tag{3}$$

which is a standard dynamical system (of size $6n$, $n$ being the number of particles) whose stability is only limited by $\|\nabla u\|^{-1} \cong \|\omega\|^{-1}$.

Such a strong stability is very useful in order to perform accurate simulations for a long time, and its Lagrangian features provide a natural approach of transport since the transport part of the Navier-Stokes equations is implicitly solved (simplified by the introduction of the characteristic curves).

This dynamical system is numerically solved by a Runge-Kutta scheme of 2nd or 4th order. The velocity and its gradient are computed by a hybrid technique:

- Vorticity carried by particle is interpolated on a grid, by means of a convolution based on a 3rd-order compact-supported kernel (Monaghan's $\mathrm{M}'_4$).
- The stream is computed on this grid, by solving a Poisson equation (in the present case in cylindrical coordinates), satisfying the no-slip-through condition.
- The velocity, i.e., the stream curl, is computed on the grid, in practice with a 4th-order centered finite-difference scheme.
- The velocity gradient and its product with the vorticity (the stretching term) are computed on the grid.
- Stretching and velocity are finally interpolated back to particles. Eq. 3 can then be advanced in time.

The details of this algorithm are fully developed in Cottet and Poncet (2003), and in its elementary formulation in Ould-Sahili, Cottet and El-Hamraoui (2000).

### Diffusion Step

The diffusion part is a heat equation on vorticity, defined on the cylindrical domain $\Omega$, which reads:

$$\begin{cases} \dfrac{\partial \omega}{\partial t} - \nu \Delta \omega = 0 \quad \text{on } \Omega \\ L(\omega) = f(\tilde{u}) \quad \text{on } \partial\Omega \\ \omega(0) = \tilde{\omega} \quad \text{on } \Omega \end{cases} \tag{4}$$

The initial condition $\tilde{\omega}$ is the final vorticity of the convection step. The boundary condition $L(\omega) = f(\tilde{u})$ aims at canceling the residual slip $\tilde{u}$ obtained after the convection step. Function $f$ is linear in $\tilde{u}$ and depends on time-step and viscosity. Operator $L$ is a tensorial differential operator of the vorticity and its flux on the body, developed in Cottet and Poncet (2003), and Poncet (2004).

Eq. 4 is itself decomposed by linearity into 2 parts:

$$\begin{cases} \dfrac{\partial \omega}{\partial t} - \nu \Delta \omega = 0 \quad \text{on } \Omega \\ L(\omega) = 0 \quad \text{on } \partial\Omega \\ \omega(0) = \tilde{\omega} \quad \text{on } \Omega \end{cases} \tag{5}$$

solved by a Particle Strength Exchange Lagrangian scheme (Degond and Mas-Gallic, 1989) in its discrete formulation, and:

$$\begin{cases} \dfrac{\partial \omega}{\partial t} - \nu \Delta \omega = 0 \quad \text{on } \Omega \\ L(\omega) = f(\tilde{u}) \quad \text{on } \partial\Omega \\ \omega(0) = 0 \quad \text{on } \Omega \end{cases} \tag{6}$$

whose solution is expressed under its integral form. The solution of this last equation has its significant values close to the body and is actually the viscous effect creating the boundary layer. (See Cottet and Poncet, 2003, for further details.)

### Validation

This method and its immersed-boundary variant have been validated in numerous test cases in early developments, including ring-vortex wall interaction (Cottet and Koumoutsakos, 2000) and 2-D wakes (Cottet and Poncet, 2002). The annular vortex and 3-D cylinder interaction involve the ring propulsion, curved boundary layer and fusion between the main ring and the boundary layer, generating a secondary ring (Cottet and Poncet, 2003; Fig. 2).

The main field of application of this numerical method was the computation of 3-D cylinder wakes, whose validation was mainly based on results by Williamson (1996) and Barkley and Henderson (1996). One can recover the main diagnostics for Reynolds numbers between 100 and 800, such as drag coefficient, Strouhal number (nondimensional frequency), 3-D instability wavelength and spectral profile (Cottet and Poncet, 2003; Poncet and Cottet, 2003; Poncet, 2004; Fig. 1). One can also recover drag curves of an impulsively started cylinder in 2-D up to Re = 9500 in the early development of the wake (Cottet and Poncet, 2002). Some topological aspects of wakes behind a cylinder into rotational oscillations have also been shown (Poncet, 2002). The typical drag and lift coefficients for an unstable cylinder wake at Re = 300 are plotted in Fig. 3.

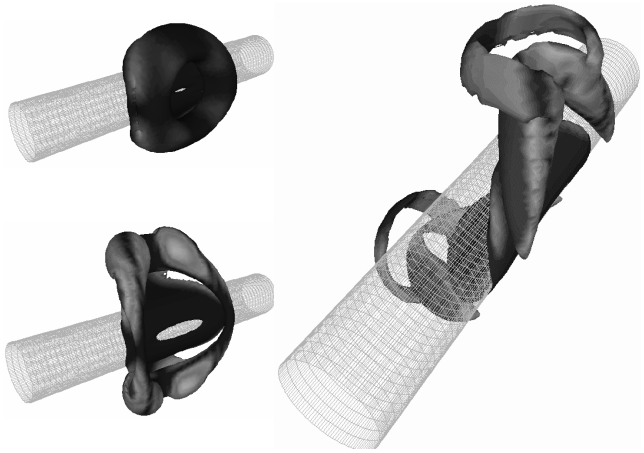

Fig. 2 Annular vortex and cylinder interaction, fusion between main ring and boundary layer, generating secondary ring-vortex (photos of vorticity at 3 different times)

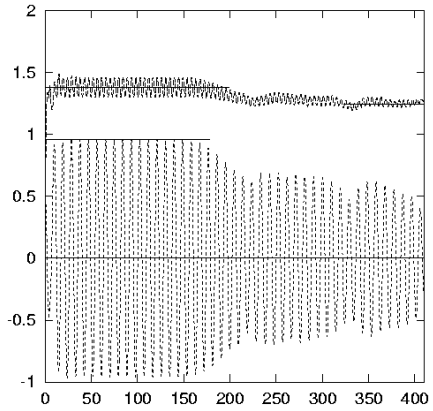


Fig. 3 Typical drag (—) and lift (- - -) coefficient of cylinder wake developing streamwise hydrodynamic instabilities at Re = 300

## OPTIMIZATION PROCESS

In order to obtain a velocity profile on the body useful for 3-D control, it is wise in a first approach to get a 2-D profile from 2-D simulations. The algorithm presented here aims at optimizing drag reduction.

### Control of 2-D Flows

One thus considers a 2-D cylinder with 16 equally long panels on the body, segments numbered from 1 to 16 (Fig. 4). Velocity profiles are thus elements in $]-b, b[^{16}$, the range $b$ being the maximum velocity allowed. This leads to an optimization problem in a control space of dimension 16, with a nonlinear cost function, whose shape is basically unknown. Genetic algorithms consequently seem a good approach in order to get close to the optimal solution.

A population of profiles is generated, and each element of the population is associated with a score based on drag reduction. Then a mutation process builds a new population where each element requires a flow computation running until an established regime is reached in order to associate a score.

Histograms plotted in Fig. 5 have been obtained by the genetic algorithm described in Milano and Koumoutsakos (2002), itself based upon the 2-D Navier-Stokes solver on a stretched O-grid by Mittal (1995). Figs. 4 and 6 give an example of the resultant flow and drag coefficient.

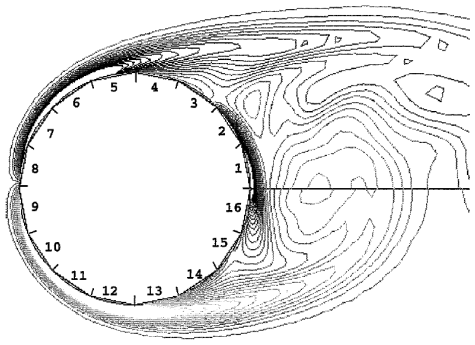


Fig. 4 Panel setup and flow example resulting from belt actuator configuration

Fig. 6 also plots (dashed line) the drag coefficient resulting from an optimization using only the 4 most significant actuators of the global optimization process, in the present case the actuators 3, 4, 13 and 14. This technique is called Clustering Genetic Algorithm (usually abbreviated as CGA, from Milano and Koumoutsakos, 2002), and provides an important gain of energy with only a minimal loss of drag reduction, thus a gain of efficiency.

### Control of 3-D Flows

In order to apply this 2-D result to 3-D simulations, one needs to use a smooth symmetric function fitting the most probable distribution of velocity obtained by the GA and CGA. Indeed, all the elements of profile population are zero mean value (and consequently the best population), but not necessarily the most probable, which is only the distribution of highest values on the histogram. The property of zero-circulation (to avoid the drag changed into lift) is required and thus the symmetry of the smooth velocity distribution. In addition, the main values of the clustered population have been used to get the smooth profile (some of

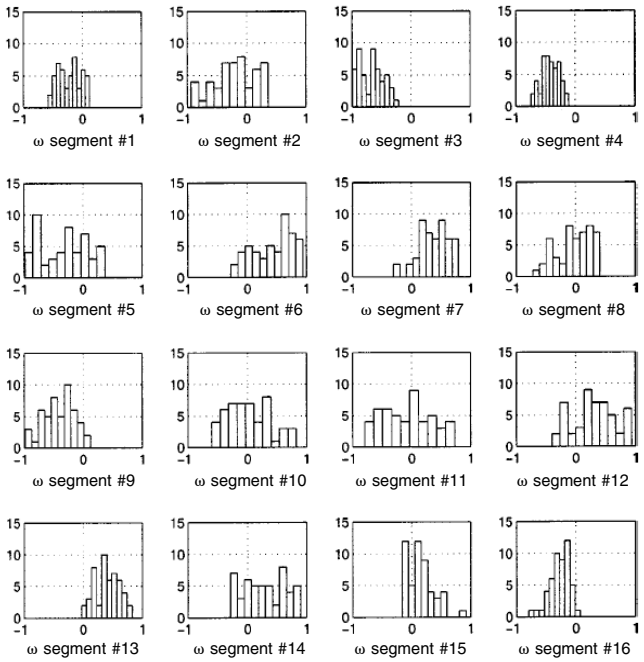


Fig. 5 Histogram of population: number of occurrences with respect to velocity values for each segment 1∼16 (Fig. 4)

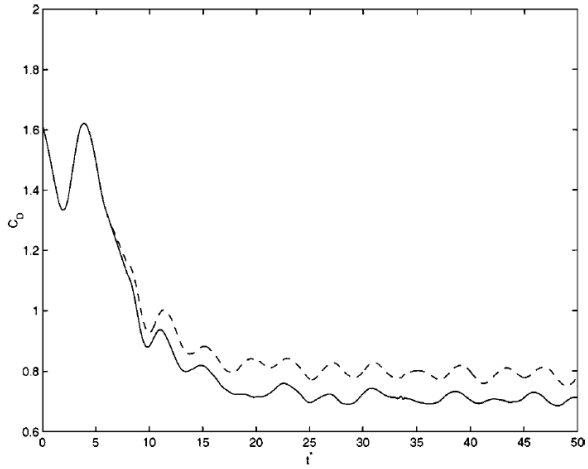


Fig. 6 Resulting drag coefficient for best populations, using all actuators (—) and only 4 most significant actuators (clustering technique, etc.)

whose significant values are plotted in Fig. 6), given in Cottet and Poncet (2004) by:

$$f(\theta) = -\sin\left(\frac{3.2\theta^3}{3+\theta^{10}}\right) \tag{7}$$

with $\theta \in ]-\pi, \pi[$.

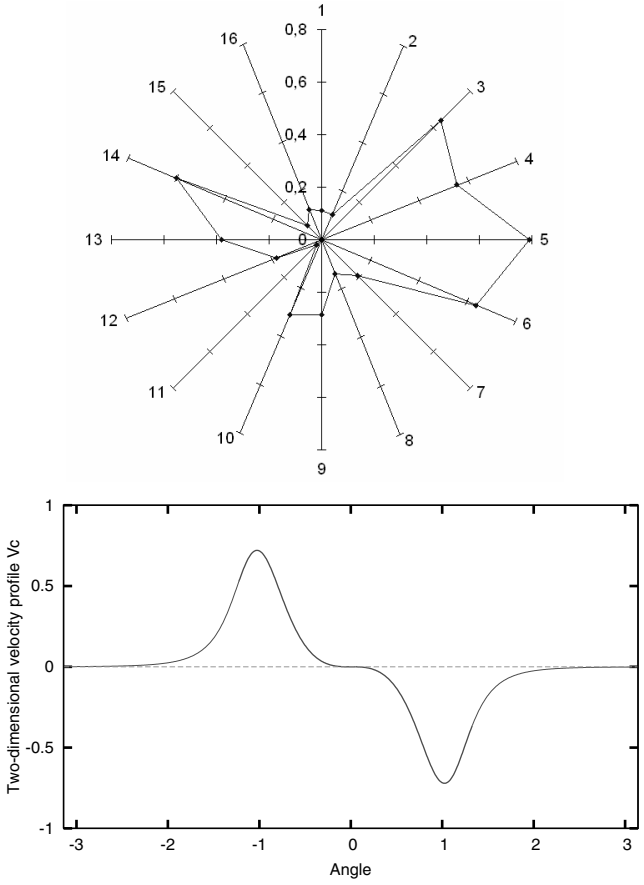


Fig. 7 Most probable velocity profile obtained with genetic algorithm (■) (top = absolute velocity with respect to segment number), and plot of fitting continuous smooth function $f(\theta)$ from Eq. 7 (bottom, velocity versus angle)

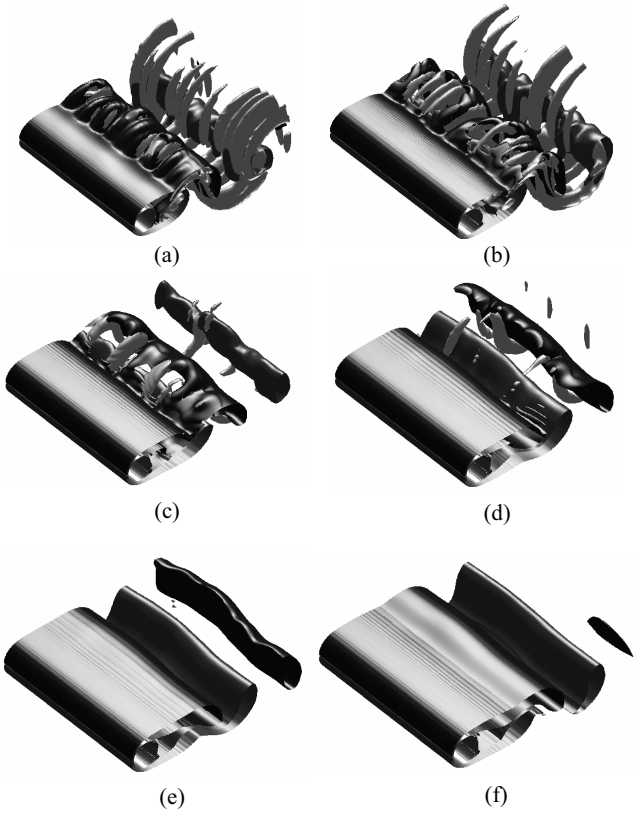


Fig. 8 Isovalues of vorticity after control activation with smooth velocity profile, at different times (a∼f, respectively, at $t = 270$, 280, 290, 300, 310 and 320), from Cottet and Poncet (2004)

The tangential velocity profile is then given by:

$$V_{\text{slip}}(\theta) = C\, f(\theta) \tag{8}$$

where $C$ is a coefficient (equal to 1 for the fitting profile—see Fig. 7) to tune the energy level involved in the control.

This smooth profile is then applied to a 3-D flow for a Reynolds number Re = 300, with streamwise hydrodynamic instabilities fully developed. In order to quantify the flow shedding, an interesting quantity is the total spanwise vorticity in a neighborhood of the body (basically the sum of the von Kármán alleys, i.e., eddies aligned with the cylinder axis), given by:

$$\Gamma_z(t) = \int_\Omega \omega_z(x, y, z, t)\, dv \tag{9}$$

The effect of the 2-D smooth velocity profile on the global spanwise vorticity of the 3-D flow, with $C = 1$, is plotted in Fig. 9,

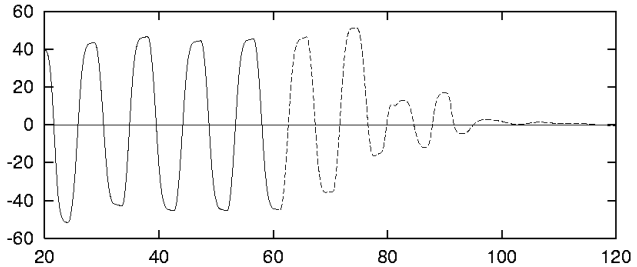

Fig. 9 Shedding (mean spanwise vorticity) before and after control activation (at $t = 60$) for 2-D control of 3-D flow

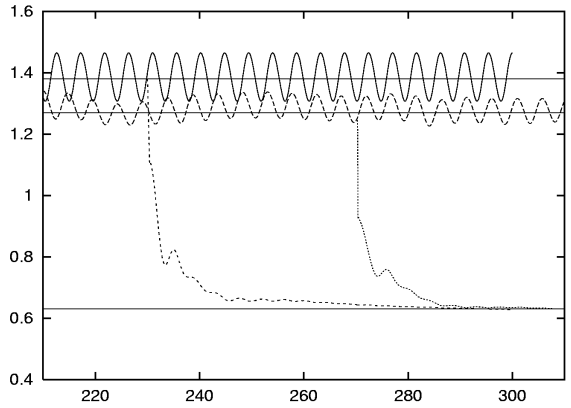


Fig. 10 Drag reduction and drag oscillation cancellation for 2-D flows (— uncontrolled, - - - controlled, activation at $t = 230$) and 3-D flows (- - uncontrolled, $\cdots$ controlled, activated at $t = 270$)

and snapshots of the 3-D isovorticity levels are given in Fig. 8. One can see that the shedding vanishes almost completely in the neighborhood of the body.

Further, since the residual shedding occurs far from the body, it does not affect the boundary layer anymore, thus also a cancellation of oscillations in the drag forces. (The resulting drag coefficient is plotted in Fig. 10.)

Another interesting property of applying tangential velocity is that the shedding reduction does not depend on the fact that the profile is 2-D or not. Indeed, when one modifies the profile into:

$$V_{\text{slip}}(\theta, z) = \frac{2C}{\sqrt{5}}(1 + \sin z) f(\theta) \tag{10}$$

then the shedding also vanishes almost completely (Fig. 11), here with a full 3-D profile ($z$ being the spanwise component). This last 3-D profile uses the same energy as the previous 2-D profile given by Eq. 8, hence a fair comparison between the 2 results.

## DEPENDENCY OF DRAG OSCILLATION VERSUS ENERGY

As seen above, the tangential velocity profile given in Eq. 8 has led, in the case of $C = 1$, to a substantial reduction of shedding in the sense of the spanwise vorticity integral in the body neighborhood (Fig. 10), accompanied by a large drop of the drag coefficient (Fig. 9), that is to say, a large difference between controlled and uncontrolled drag coefficients. The reference is the drag coefficient of the 3-D uncontrolled flow, 1.262 from Cottet and Poncet (2003). Plus, one may note that large energies may lead to a complete loss of the von Kármán eddies structuring the uncontrolled flow (Fig. 12).

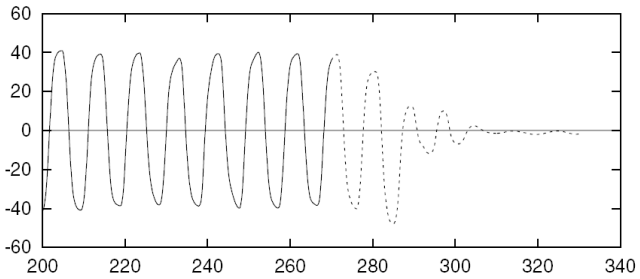


Fig. 11 Shedding (mean spanwise vorticity) before and after control activation (at $t = 270$) for 3-D control of 3-D flow

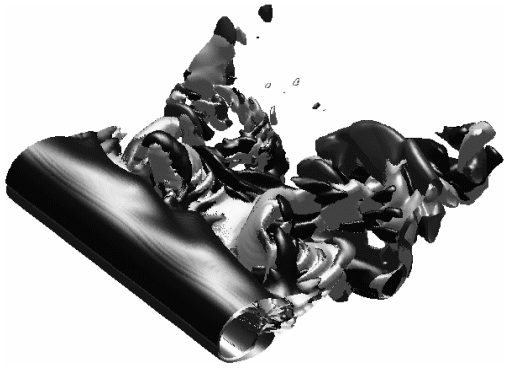

Fig. 12 Effect of 3-D control of 3-D flow at large energies and large wavelength (locked on mode A)

Since the drag and lift forces are given by the drag and lift coefficients, a study of oscillations of these quantities, especially the drag coefficient, would clarify how the shedding reduction is linked to the energy involved in the control. Eq. 8 implies:

$$E_c = \int_\Omega V_{\text{slip}}(\theta)^2 d\theta = C^2 \int_\Omega f(\theta)^2 d\theta \tag{11}$$

thus kinetic energy involved to enforce the velocities on the body behaves as $C^2$. It has been noticed in the past that the pressure part of the drag coefficient is a linear function of the radial derivative of vorticity (Cottet and Koumoutsakos, 2002; Cottet and Poncet, 2003), itself a linear function of the residual velocity at the end of the convection step given by Eq. 3. This spurious velocity is in practice a fraction of the velocity imposed on boundary.

Consequently, one can expect a linear behavior between the drop of drag coefficient and the boundary velocity amplitude $C$. In addition, the kinetic energy is quadratic in $C$, by means of Eq. 11. Thus, we strongly expect to observe a square-root regression of the drop of mean drag coefficient with respect to the kinetic energy involved in the control. This fact is indeed observed and plotted in Figs. 13 and 14, in standard and logarithmic scales, for various values of $C$.

Once the behavior of drag reduction with respect is identified, it is thus possible to study the deviation of the drag coefficient

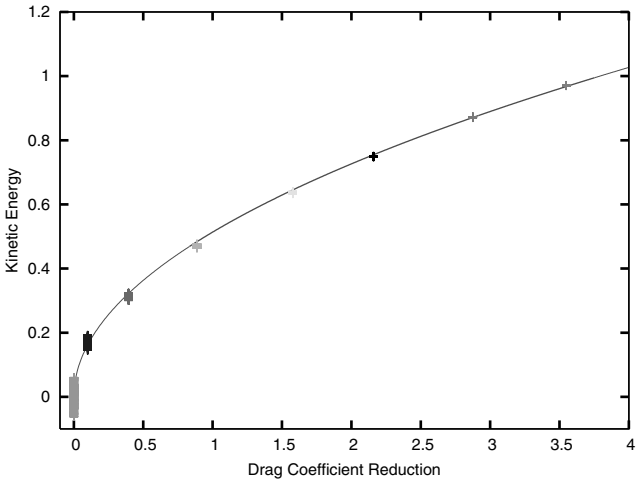


Fig. 13 Drag coefficient reduction versus kinetic energy, for various values of $C$ (left to right: 0, 0.25, 0.5, 0.75, 1, 1.17, 1.35 and 1.5) and its square-root regression

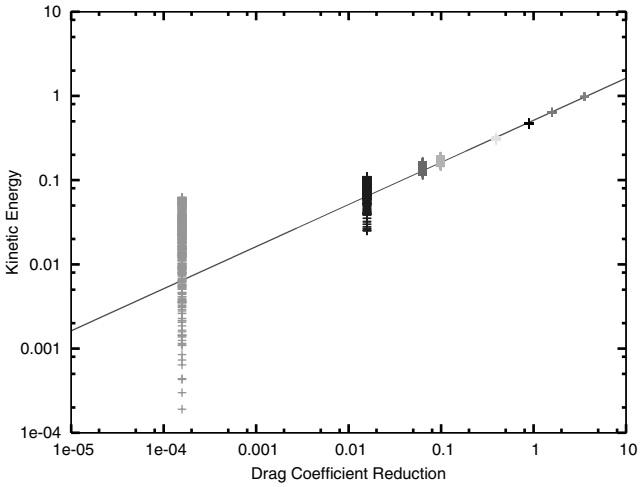


Fig. 14 Drag coefficient reduction versus kinetic energy in logarithmic scale, for various values of $C$ (left to right: 0.01, 0.1, 0.2, 0.25, 0.5, 0.75, 1 and 1.5) and its square-root regression

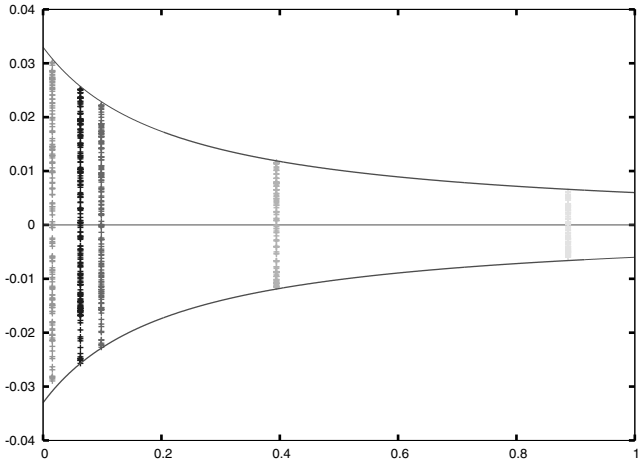


Fig. 15 Shedding reduction: drag coefficient (deviation from mean value) versus kinetic energy in low-energy control (small values of $C$) and its fitting curve

(force oscillation) from its mean value. For small energies, this deviation is plotted in Fig. 15, in which the oscillation follows seemingly an inverse polynomial law for energies below 1:

$$\max|\Delta C_D| \cong 0.033(1+4.5E_c)^{-1} \tag{12}$$

For larger energies (up to 4—Fig. 16), one observes a slower decreasing property:

$$\max|\Delta C_D| \cong 0.06(1+13E_c)^{-0.9} \tag{13}$$

Still, for both cases, the oscillation amplitude is roughly proportional to the inverse of kinetic energy involved in the control.

Further, one can also check that the drag oscillation is a good representative of force oscillation. Indeed, as shown in Figs. 17 and 18, the lift oscillations decrease as the drag no longer oscillates.

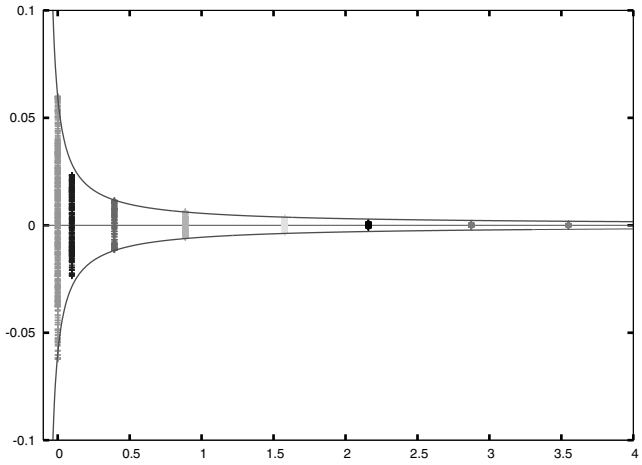


Fig. 16 Same as Fig. 15 for larger values of $C$

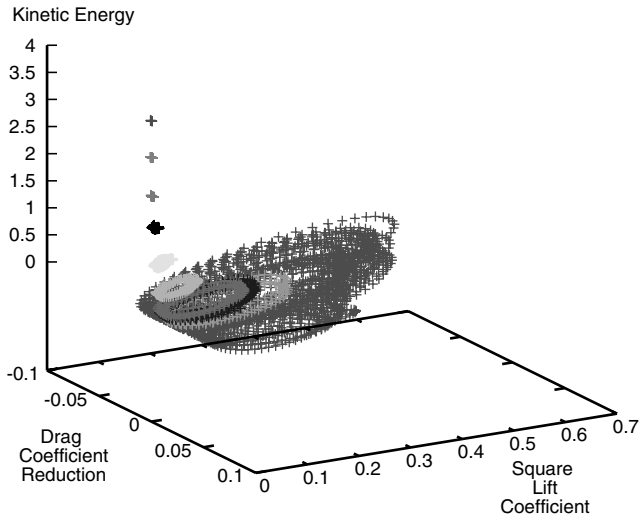


Fig. 17 Attractor: Drag coefficient/lift coefficient/energy (Eq. 11)

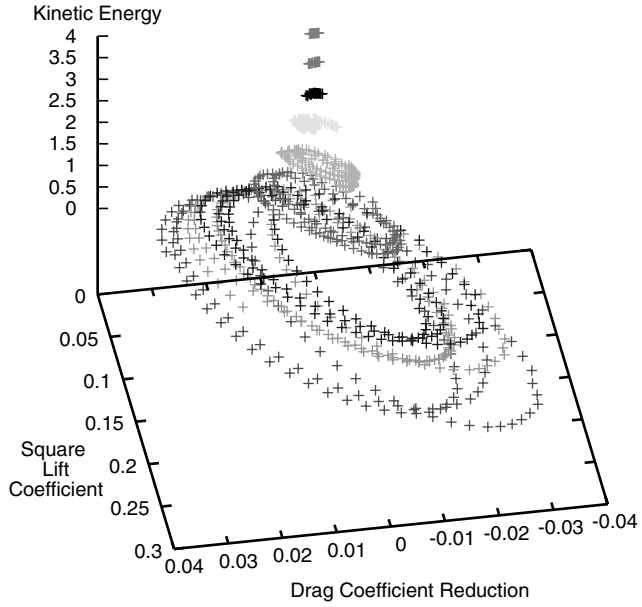


Fig. 18 Same as Fig. 17 without uncontrolled data

## CONCLUSION

A clustering genetic algorithm has been used to build a quasi-optimal 2-D profile of tangential velocities on a cylindrical body. The optimality is in the sense of the drag coefficient optimization.

This profile is then applied to a 3-D flow in order to study the effect of such a control on 3-dimensionality and realistic drag coefficient. In order to avoid a lack of regularity (and thus a lack of accuracy), the profile obtained by the genetic algorithm is smoothed. The flow is computed by a robust vortex-in-cell method in order to reach long time scales, computed over a large domain, with small wavelength instabilities to compute accurately.

These simulations have shown that the mean drag coefficient behaves as a square-root function of the energy involved in the control, and the force oscillations (shedding) decrease as the inverse of energy.

Another quantity measuring the shedding is the amount of spanwise vorticity in the body neighborhood. This quantity is intrinsic to the flow and is not related to forces, but gives a good idea of how the flow oscillates. It exhibits a sharp drop when control is activated and shows that shedding almost completely vanishes. The same behavior has been observed when control is fully 3-D, which means that the shedding reduction may not depend on the spanwise-constant property of the tangential velocity profile, but only on the energy involved, at least for large energies.

Tangential actuators, such as the model belt actuators proposed here, offer the advantage that when inactive they do not add to the drag of the system. The incorporation of such actuators in engineering systems can offer a multitude of synergetic control possibilities, through their spatial arrangement and the time-dependence and schedule of their activation.

## ACKNOWLEDGEMENTS

The authors would like to thank Georges-Henri Cottet for his participation during the development of this work. We also would like to acknowledge the computational support of CEA-CENG (Grenoble, France).

## REFERENCES

Barkley, D, and Henderson, RD (1996). "Three Dimensional Floquet Stability Analysis of the Wake of a Circular Cylinder," *J Fluid Mech*, Vol 332, pp 215–241.

Cottet, G-H, and Koumoutsakos, P (2000). *Vortex Methods, Theory and Practice*, Cambridge University Press.

Cottet, G-H, and Poncet, P (2004). "New Results in the Simulation and Control of Three-dimensional Cylinder Wakes," *Comput Fluids*, Vol 33, pp 697–713.

Cottet, G-H, and Poncet, P (2003). "Advances in Direct Numerical Simulations of Three-dimensional Wall-bounded Flows by Vortex-in-Cell Methods," *J Comp Phys*, Vol 193, pp 136–158.

Cottet, G-H, and Poncet, P (2002). "Particle Methods for Direct Numerical Simulations of Three-dimensional Wakes," *J Turbulence*, Vol 3, No 38, pp 1–9.

Degond, P, and Mas-Gallic, S (1989). "The Weighted Particle Method for Convection-diffusion Equations," *Math Comput,* Vol 53, pp 485–526.

Milano, M, and Koumoutsakos, P (2002). "A Clustering Genetic Algorithm for Cylinder Drag Optimization," *J Comp Phys*, Vol 175, pp 79–107.

Mittal, R (1995). "Large-Eddy Simulation of Flow Past a Circular Cylinder," *Annual Res Briefs*, Center for Turbulence Res, p 107.

Ould-Sahili, ML, Cottet, G-H, and El Hamraoui, M (2000). "Blending Finite-differences and Vortex Methods for Incompressible Flow Computations," *SIAM J Sci Comput*, Vol 22, pp 1655–1674.

Poncet, P (2004). "Topological Aspects of Three-dimensional Wakes Behind Rotary Oscillating Circular Cylinders," *J Fluid Mech*, Vol 517, pp 27–53.

Poncet, P, and Cottet, G-H (2003). "Open-loop Control of Three-dimensional Wakes," *Proc 2nd MIT Conf,* Vol 2, pp 2348–2351.

Poncet, P (2002). "Vanishing of Mode B in the Wake Behind a Rotationally Oscillating Circular Cylinder," *Phys Fluids*, Vol 14, No 6, pp 2021–2024.

Williamson, CHK (1996). "Three-dimensional Wake Behind a Cylinder," *J Fluid Mech*, Vol 328, p 345.